

Comparative photodecolorization of red dye by anatase, rutile (TiO_2), and wurtzite (ZnO) using response surface methodology

Shahab Khameneh ASL^{1,2,3}, Sayad Khatib SADRNEZHAAD⁴,
Mansour Keyanpour RAD², Deniz ÜNER^{1,*}

¹*Department of Chemical Engineering, Middle East Technical University,
İnönü Bulvarı, 06531 Ankara-TURKEY
e-mail: uner@metu.edu.tr*

²*On leave: Department of New Materials, Materials and Energy Research Center,
Tehran-IRAN*

³*On leave: Faculty of Mechanical Engineering, University of Tabriz, Tabriz-IRAN*

⁴*Center of Excellence for Advanced Processes of Production of Materials,
Department of Materials Science and Engineering, Sharif University of Technology, Tehran-IRAN*

Received: 12.04.2011

Treatment of dye pollution containing C.I. Acid Red 14 (AR14) by a coupled photocatalytic process was studied. Titanium dioxide, in the form of anatase and rutile, and zinc oxide, were used as photocatalysts. The investigated photocatalysts were Aldrich-produced nanopowders with crystallites of a mean size of 20-30 nm and a specific surface area of about 50 m²/g. A comparison of $\text{TiO}_{2(\text{anatase})}$, $\text{TiO}_{2(\text{rutile})}$, $\text{TiO}_{2(a,r)}$, and ZnO for the decolorization of the AR14 solution was performed. Results showed that color removal followed the decreasing order of $\text{TiO}_{2(a,r)}$, ZnO > $\text{TiO}_{2(a,r)}$ > $\text{TiO}_{2(a)}$, ZnO > $\text{TiO}_{2(r)}$, ZnO > $\text{TiO}_{2(a,r)}$ > $\text{TiO}_{2(a)}$ > ZnO > $\text{TiO}_{2(r)}$. Response surface methodology (RSM) was employed to assess the individual and interactive effects of the 4 main independent parameters in the photocatalytic process. Analysis of variance showed a high coefficient of determination ($R^2 = 0.9396$) and satisfactory prediction second-order regression. The optimum initial amounts of $\text{TiO}_{2(a)}$, $\text{TiO}_{2(r)}$, ZnO, and dye and the reaction time were found to be 84 ppm, 23 ppm, 86 ppm, 20 ppm, and 48 min, respectively. It was demonstrated that RSM with suitable 2D and 3D graphs was a suitable method for finding the interactions between parameters, identifying the main parameters, and optimizing the operating conditions.

Key Words: ZnO nanoparticles, TiO_2 nanoparticles, experimental design, response surface methodology, photocatalysis

*Corresponding author

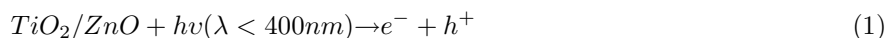
Introduction

Water-pollution control is an active research area because colored organic compounds released from the paper, plastic, textile, and dyestuff industries are causing significant problems for human health and aquatic life.¹ Over 100,000 commercially available dyes exist, and more than 7×10^5 t are produced annually.² Among many of the physical and chemical removal systems for dyes recently developed,^{3,4} the application of advanced oxidation processes (AOP), especially photocatalysis using a semiconductor nanoparticulate system,⁵ appears to be the most favorable treatment when compared to the more traditional chemical decomposition processes. This is because most of the ceramic semiconductors offer high absorption and surfaces areas,⁶ which can be adjusted with preparation parameters. Furthermore, they are cheap and nontoxic. They can contribute to the decomposition reaction in different ways without decreasing their activity over time. Furthermore, particles could be recovered by filtration or centrifugation, or could be fixed in fluidized bed reactors.⁶

In photocatalytic reactions, pure or doped ceramic semiconductors (e.g. TiO_2 , ZnO , WO_3 , CdS , CdSe , Nb_2O_5 , SrTiO_3 , or Ag-doped TiO_2) are commonly used as catalysts.⁷ The main step in photoreaction is the formation of electron-hole pairs upon irradiation with the proper photon energy to overcome the band gaps. When the energy is larger than the band gap, the electron-hole pairs are separated between the semiconductor's valance and conduction bands. The adsorbed species (reactants) on suitable sites on the surface of the catalyst undergo photooxidation, reduction, or synthesis. Ultraviolet (UV) light, sunlight, or ultrasonic sources are commonly used for this purpose.⁸

The steps of the photocatalytic process using TiO_2 or ZnO as a catalyst can be written as follows.⁹

1. Charge carrier generation:



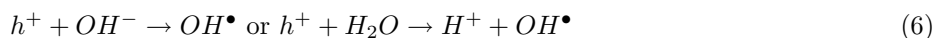
2. Charge trapping in the particles, especially on the surface:



3. Charge recombination:



4. Interfacial charge transfer:



The hydroxyl radical or the directly produced charge is a powerful oxidizing agent and attacks dyes present at or near the surface of the semiconductor. It ultimately causes the complete degeneration of the dye into harmless compounds.

The 2 principal catalytic phases of TiO_2 , anatase (3.2 eV) and rutile (3.0 eV), have numerous structural and functional differences.^{9–12} The adsorptive affinity of anatase for organic compounds like dye is higher than that of rutile, and anatase is generally regarded as the more photocatalytic active phase of titanium oxide, presumably due to the combined effect of lower rates of recombination and higher surface sites.¹³ ZnO, the other semiconductor (3.2 eV), appears to be a suitable alternative to TiO_2 since its photooxidation mechanism is similar to that of TiO_2 .^{14,15} ZnO has been reported, in some cases such as the photooxidation of 2-phenylphenol or phenol, to be more efficient than TiO_2 .¹⁴ The efficiency of the photocatalytic oxidation of semiconductors could be increased by coupling 2 phases;¹⁶ a sample of this behavior was seen in P25 titania, which contains anatase and rutile with more efficient electron-hole separation^{13,17} and photocatalytic sites.

In this study, we optimized the removal of AR14 as a model dye from aqueous solutions using the coupled photocatalytic process. To the best of our knowledge, the systematic optimization of photocatalytic decolorization of AR14 solution by UV/ $\text{TiO}_{2(a)}$, $\text{TiO}_{2(r)}$, and ZnO has not been reported before. Response surface methodology (RSM) was used to study the influence of catalyst phases on the decolorization efficiency of AR14. The percent decolorization (%) was used as the response for optimization, and the mathematical relationship between the parameters and the most important factors was established.

Materials and methods

Chemicals

Acid Red 14 dye, with the formal IUPAC chemical name of disodium (E)-4-hydroxy-3-((4-sulfonatophthalen-1-yl)diazenyl)naphthalene-1-sulfonate ($\text{C}_{20}\text{H}_{12}\text{N}_2\text{Na}_2\text{O}_7\text{S}_2$), was obtained from Rang Azar Company, Iran. Its structure and characteristics are given in Table 1. Analytical grade nanopowders of $\text{TiO}_{2(a)}$, $\text{TiO}_{2(r)}$, and ZnO were obtained from Sigma-Aldrich, Germany. The specific surface area of the powders was about $50 \text{ m}^2/\text{g}$ and the particle size of the powders was about 20-30 nm, according to the specifications of the manufacturers.

Instruments

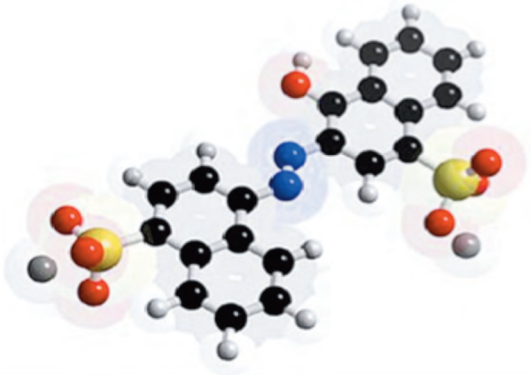
Scanning electron microscopy (SEM) of the catalysts was carried out on a Cambridge Stereoscan S-360 device (Leica, California, USA) after gold CVD coating. The removal of color was followed by using a UV-Vis spectrophotometer (PG Instruments T80⁺, China). Before the analysis of samples extracted from solutions, the solutions were filtered with an AIM nylon syringe filter, 13 mm in diameter with a pore size of $0.2 \mu\text{m}$. The irradiation source was a 100-W UV-A lamp (UVP, Inc., California, USA) with a maximum wavelength of 365 nm.

Photoreactor

The experiments were performed in a batch photoreactor with a volume of 200 mL and an upper light source. Solutions containing 20 ppm of dye and known concentrations of catalysts were prepared and transferred to the reactor. The light source was then turned on while the suspension was agitated to keep the system homogeneous. The concentration of dye at the initial condition and each appropriate time was determined with a UV-Vis

spectrophotometer at $\lambda_{max} = 515$ nm. The decolorization efficiency (CR%) was expressed as the percentage ratio of the decolorized dye concentration to that of the initial concentration.

Table 1. Characteristics of C.I. Acid Red 14.

Molecular formula	Disodium (E)-4-hydroxy-3-((4-sulfonatophthalen-1-yl)diazenyl)naphthalene-1-sulfonate (C ₂₀ H ₁₂ N ₂ Na ₂ O ₇ S ₂)
Color index number	14,720
λ_{max} (nm)	515
Molecular weight (g/mol)	502.43
Chemical structure	

Experimental design

In the present study, the central composite design (CCD) form of RSM was used for the optimization of parameters. To evaluate the influence of reactor parameters on the decolorization, 4 main factors and 3 levels were selected: initial TiO_{2(a)} concentration (a), initial TiO_{2(r)} concentration (r), initial ZnO concentration (z), and reaction time (t). A total of 31 experiments were introduced with Minitab 15 software, including 2⁴ =16, 7, and 8 points as the cube, replications at the center, and axial conditions, respectively.¹⁸⁻²⁰ For statistical calculations, the variables X_i were transformed to nondimensional codes as x_i, according to the following relationship:

$$x_i = \frac{X_i - X_o}{\delta X} \quad (8)$$

where X_o is the value of X_i at the center point and δX is the step change.¹⁸ The experimental ranges and the levels of the independent variables for this set-up are presented in Table 2.

Table 2. Experimental ranges and levels of the independent test variables.

Variables	Ranges and levels				
	-2	-1	0	+1	+2
Anatase concentration (ppm) (a)	20	40	60	80	100
Rutile concentration (ppm) (r)	20	40	60	80	100
ZnO concentration (ppm) (z)	20	40	60	80	100
Reaction time (min) (t)	20	40	60	80	100

Results and discussion

Catalyst structural characterization

Figure 1 shows the SEM image of the nanoparticles. The zinc oxide and titanium oxide powders have cubic-like and spherical microstructures with similar particle size ranges, which are in agreement with the specific surface areas and particle sizes reported by the manufacturer.

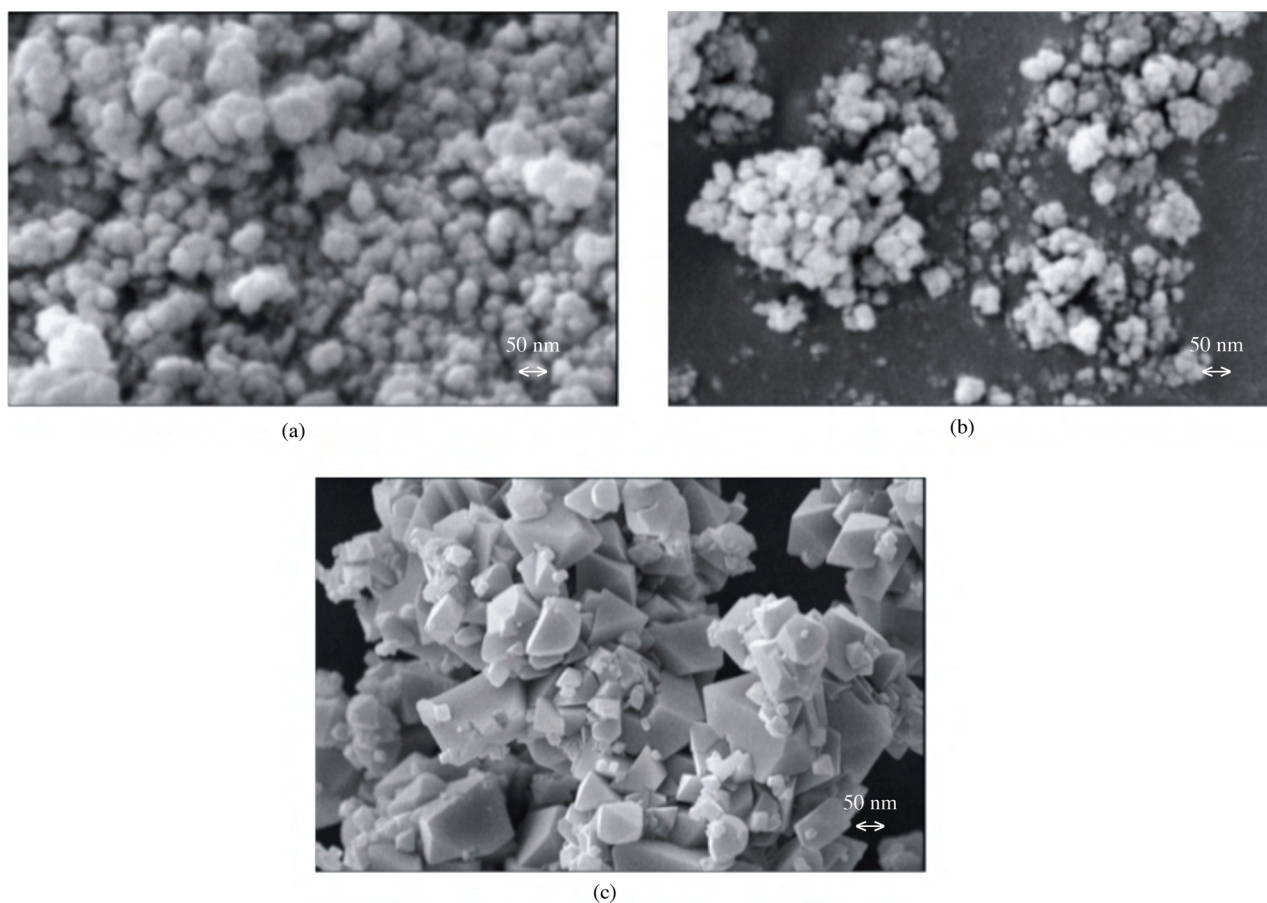


Figure 1. Scanning electron microscopy images of the nanoparticles: a) anatase, b) rutile, c) ZnO.

Decolorization of AR14 by single photocatalyst process

The concentration of the dye in solution versus UV-VIS intensity at 515 nm was calibrated and the results are presented in Figure 2. A comparison of single $\text{TiO}_{2(a)}$, $\text{TiO}_{2(r)}$, and ZnO photocatalytical decolorization of the solution containing AR14 was performed. Figure 3a shows the removal efficiency for a 20-ppm AR14 solution by a 100-ppm catalyst at room temperature (25 °C). It can be observed that the highest removal efficiency was obtained using $\text{TiO}_{2(a)}$. The reaction rate (slope) also indicates that dye removal efficiency followed the decreasing order of $\text{TiO}_{2(a)} > \text{ZnO} > \text{TiO}_{2(r)}$. Furthermore, the dye decolorization treatment displayed a pseudo-first-order kinetic behavior, as seen in Figure 3b. The specific reaction rate for $\text{TiO}_{2(a)}$ was 0.0304 min^{-1} , whereas, under the same conditions, the specific rates for $\text{TiO}_{2(r)}$ and ZnO were 0.0082 and 0.0254 min^{-1} , respectively. These results indicate that anatase (3.2 eV) and wurtzite (3.2 eV) have higher photocatalytic activities than rutile (3.0 eV).

Central composite design model

In statistics, a central composite design, also known as the Box-Wilson design, is an experimental design methodology for building a second-order (quadratic) model for the response variable without needing to use a complete 5-level factorial experiment.¹⁹ It has 3 steps: selecting the design, predicting coefficients, and checking adequacy.²¹ The 4-factor, 5-level CCD matrix and experimental results of the process are presented in Table 3. A second-order polynomial equation was used to express the decolorization percentage as a function of independent variables.²²

$$Y = B_0 + B_1a + B_2r + B_3z + B_4t + B_{12}ar + B_{13}az + B_{14}at + B_{23}rz + B_{24}rt + B_{34}zt + B_{11}a^2 + B_{22}r^2 + B_{33}z^2 + B_{44}t^2, \quad (9)$$

where Y is the measured response, a_0 is the intercept term, $B_{1,2,3,4}$ are the linear coefficients, $B_{12,13,14,23,24,34}$ are the logarithmic coefficients, $B_{11,22,33}$ are the quadratic coefficients, and r, a, z, and t are coded independent variables. Low and high factor settings were coded as -2 and 2, and the midpoint was coded as 0.

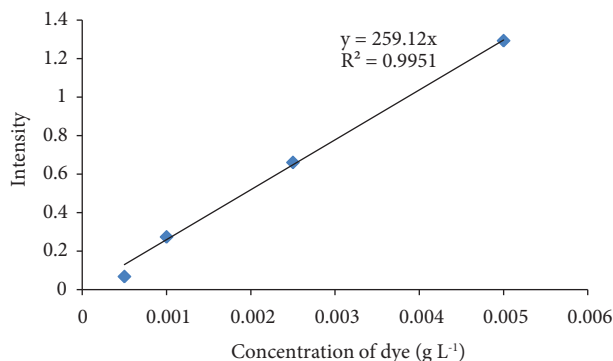


Figure 2. Calibration curve of dye concentration versus UV-Vis spectral intensity at 515 nm.

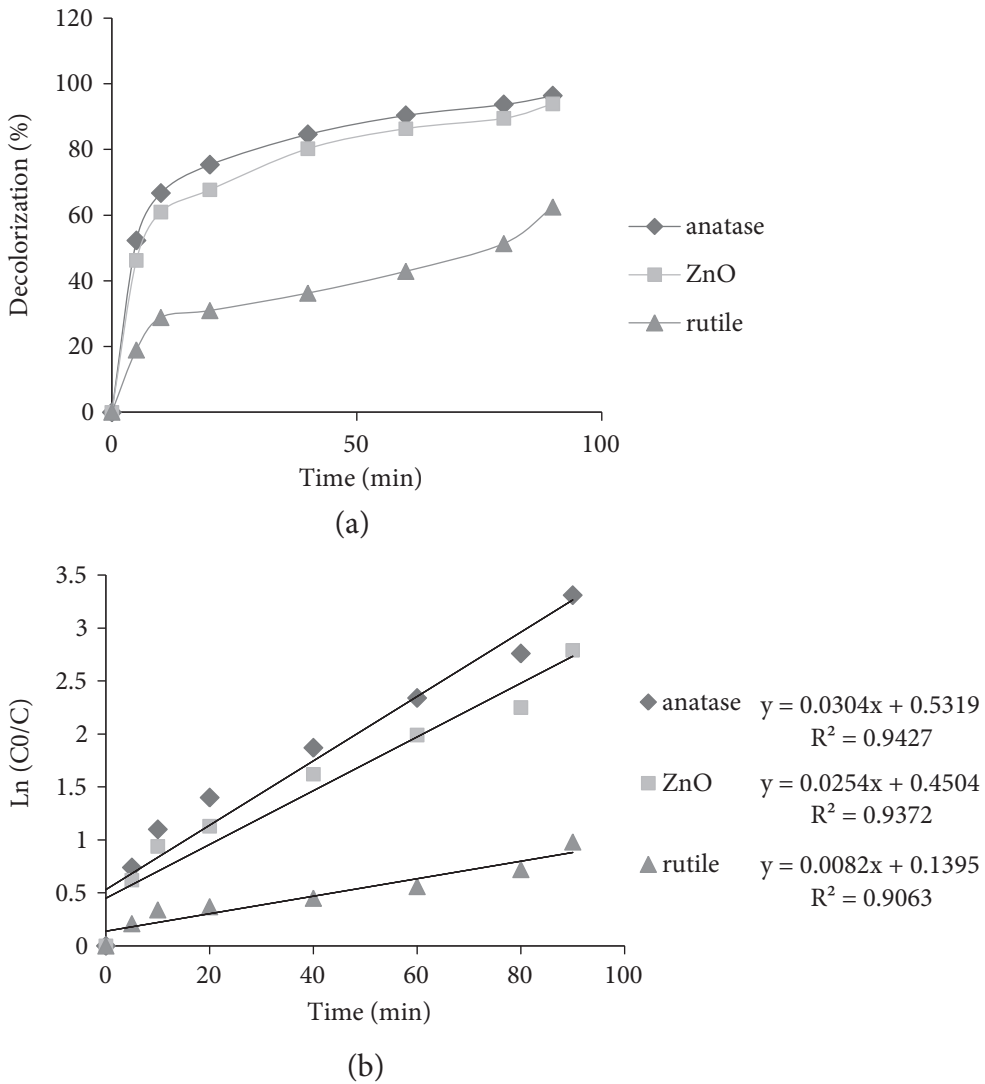


Figure 3. a) Removal efficiency (CR%) and b) decolorization rate (min^{-1}) for a 20-ppm AR14 solution using a 100-ppm catalyst at room temperature.

After running the 31 trials, an empirical relationship between the Y and independent variables (a, r, z, and t) was determined as the following second-order polynomial equation:

$$\begin{aligned}
 Y = & -31.4066 + 0.9778a + 0.3397r + 0.5293z + 0.4723t - 0.0048ar + 0.0009az - 0.0028at - 0.0003rz \\
 & + 0.0002rt - 0.0036zt - 0.0008a^2 + 0.0028r^2 + 0.0007z^2 + 0.0014t^2.
 \end{aligned}
 \tag{10}$$

The decolorization percentages predicted by Eq. (10) and the experimental results are shown to be in good agreement with each other in Table 3.

Table 3. The 4-factor central composite design matrix and the value of response function (CR%).

Run	Anatase (ppm)	Rutile (ppm)	ZnO (ppm)	Time (min)	Decolorization efficiency (%)	
					Experimental	Predicted
1	60	100	60	60	77	78
2	80	80	80	40	90	90
3	20	60	60	60	53	55
4	60	60	60	60	74	75
5	60	60	20	60	59	59
6	40	80	80	40	78	72
7	60	60	60	60	74	75
8	80	40	80	40	90	92
9	80	80	40	40	71	70
10	80	80	40	80	80	81
11	60	60	100	60	94	93
12	100	60	60	60	95	92
13	60	60	60	60	75	75
14	80	80	80	80	95	96
15	80	40	40	80	80	82
16	60	20	60	60	74	72
17	40	80	40	40	50	53
18	80	40	80	80	97	97
19	60	60	60	60	74	75
20	40	40	80	40	64	66
21	40	40	40	40	50	46
22	80	40	40	40	70	71
23	60	60	60	100	90	88
24	60	60	60	60	76	75
25	40	80	40	80	74	69
26	60	60	60	60	75	75
27	60	60	60	20	65	66
28	60	60	60	60	75	75
29	40	80	80	80	79	83
30	40	40	40	80	59	62
31	40	40	80	80	78	76

Checking the model

To confirm the goodness of fit of the model and the experimental results, regression coefficient (R-squared) analysis was applied and is shown in Figure 4. According to the R-squared value, which is close to 1.0 (minimizing the square of errors), the regression line is perfectly fitted with the experimental points. This indicates that the value of the equation is useful to predict the results at specific points with an accuracy of about 96.78%. This model could also be used to predict the decolorization percentage at other catalytic contents and times.

The adjusted R^2 is a modification of R^2 that adjusts for the number of explanatory terms in a model.^{18,19} Unlike R^2 , the adjusted R^2 increases only if the new term improves the model more than would be expected by chance. The adjusted R^2 can be negative, and it will always be less than or equal to R^2 . The adjusted R^2 is more suitable for comparing models with different numbers of parameters, like in the present study. Here, the adjusted R^2 value (0.9396) is similar to R^2 and close to 1.0 (perfect condition).

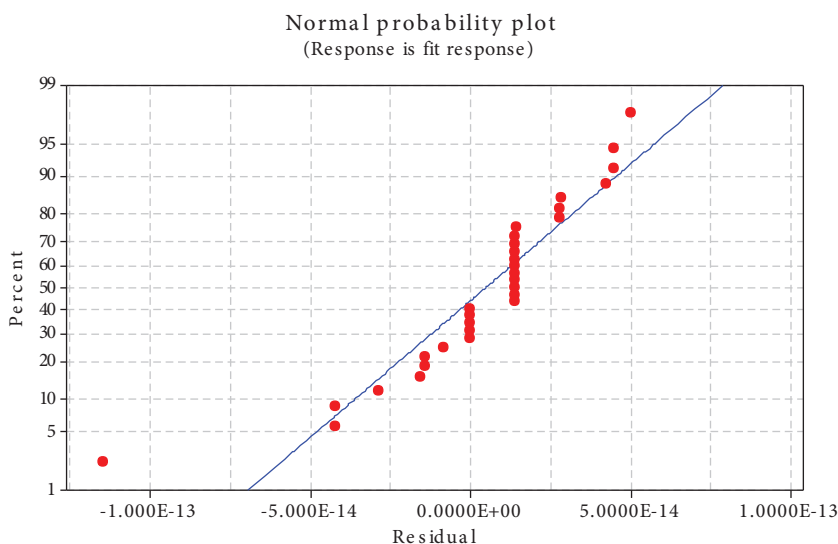


Figure 4. Normal plot of probability of experimental values via predicted output.

The regression mathematical model was tested for statistical significance using analysis of variance (ANOVA). ANOVA is a collection of statistical models and their associated procedures, in which the observed variance in a particular variable is partitioned into components attributable to different sources of variation.²³

In Table 4, statistical results are shown that summarize the sum of squares of residuals and regressions together with the corresponding degrees of freedom, F-values, P-values, and ANOVA coefficients. The mathematical relations applied for calculation of the ANOVA estimators are widely presented in the literature concerning response surface methodology.^{24,25}

ANOVA is composed of 2 sources: variation associated with the model and variation associated with the experimental error, and the F-value shows the ratio of these 2, using the significance of the model. If the F-value is greater than the value of the F-distribution for a certain number of degrees of freedom in the model at level of significance α , the model is perfectly fit.¹⁹

Table 4. Analysis of variance (ANOVA) for fit of decolorization efficiency from central composite design.

Source of variations	Sum of squares	Degree of freedom	Adjusted mean square	F-value	P-value
Regression	4748.39	14	339.1705	34.31	0.000
Linear	4617.85	4	36.5261	3.70	0.026
Square	15.05	4	3.7632	.38	0.819
Interaction	115.49	6	19.2477	1.95	0.134
Residuals	158.15	16	9.8841		
Lack of fit	153.66	10	15.3658	20.54	0.001
Pure error	4.49	6	0.7481		
Total	4906.53	30			

$R^2 = 0.9678$; adjusted $R^2 = 0.9396$.

P-values were applied to check the significance of each of the coefficients, which are necessary to understand the pattern of the mutual interactions between the test variables. The larger the magnitude of the t-value

and the smaller the P-value, the more significant the corresponding coefficient is. These values are presented in Table 5.

Table 5. Estimated regression coefficients and corresponding t- and P-values from the data of the central composite design experiments.

Coefficient	Parameter estimate	Standard error	t-value	P-value
B ₀	-31.4066	20.9472	-1.499	0.153
B ₁	0.9778	0.2717	3.598	0.002
B ₂	0.3397	0.2717	1.250	0.229
B ₃	0.5293	0.2717	1.948	0.069
B ₄	0.4723	0.2717	1.738	0.101
B ₁₂	-0.0008	0.0016	-0.573	0.576
B ₁₃	0.0002	0.0015	0.161	0.874
B ₁₄	0.0007	0.0016	0.469	0.645
B ₂₃	0.0014	0.0016	0.930	0.366
B ₂₄	-0.0048	0.0020	-2.459	0.026
B ₃₄	0.0009	0.0020	0.439	0.667
B ₁₁	-0.0028	0.0020	-1.438	0.170
B ₂₂	-0.0003	0.0020	-0.157	0.877
B ₃₃	0.0002	0.0020	0.122	0.904
B ₄₄	-0.0036	0.0020	-1.827	0.086

Pareto analysis is a formal technique useful where many possible courses of action are competing for attention. In essence, the problem solver estimates the benefit delivered by each action, then selects a number of the most effective actions that deliver a total benefit reasonably close to the maximal possible one.¹⁸ In this case, it indicates the percentage effect of each factor on the response, according to the following relation:

$$P_i = \left(\frac{B_i^2}{\sum B_i^2} \right) \times 100 \quad (i \neq 0). \quad (11)$$

Pareto analysis graphic analyses are summarized in Figure 5. The results suggest that the most important parameters are B₁, B₂, and B₃, which represents the fact that the effects of single phases are high. In coupled conditions (B₁₂, B₁₃, B₁₄, B₂₃, and B₂₄, which show the effect of 2 phases simultaneously), however, the effects are low. These results indicate that adding 2 or 3 semiconductors to the system has no coupling effect because oxide particles, which are in the parts-per-million range, covered by dielectric (water) atoms, and producing electrons and holes that are stable for only nanoseconds,^{9,26} could not pass from one semiconductor to another to effectively separate and create a delay in the recombination rate and an increase in photocatalytic activities.¹⁶ The main advantages of using 2 or 3 kinds of photocatalysts with similar band gaps are overcoming solution limitations and adding new and different site locations to react with dye.⁹

Response surface and counter plots

In order to visualize the effect of every 2 variables while 2 other parameters are kept constant, 3D and contour (2D) plots of predicted responses are shown in Figures 6 and 7. These graphs are plotted based on the model, interpolating the points to the lines and the surfaces.

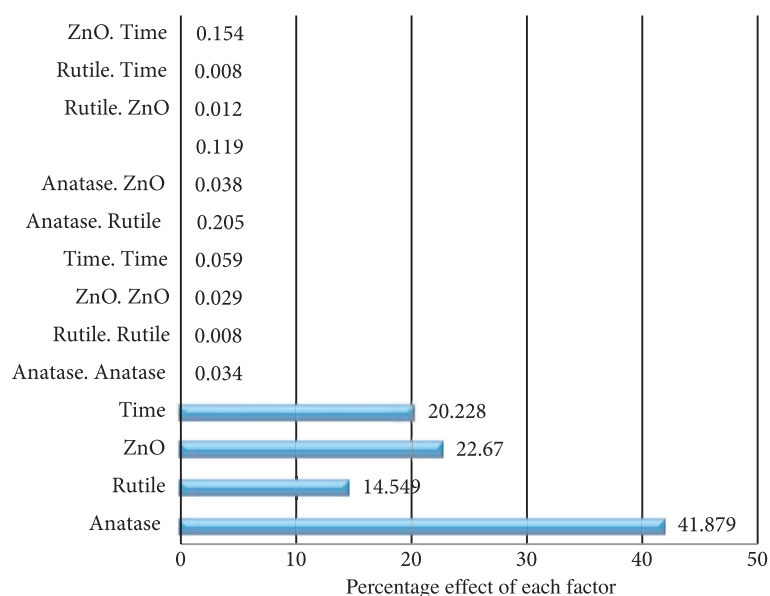


Figure 5. Pareto graphical analysis.

The response surface and contour plots were developed as a function of reaction time and anatase, rutile, and wurtzite concentrations, respectively, and are shown in Figure 6, while 2 other factors were fixed at central levels. As can be seen in Figure 6, decolorization efficiency increases with increasing reaction time in all graphs. On the other hand, the decolorization efficiency increased with the increase of catalyst concentration. The rate of decolorization related to the anatase sample was higher than that for both wurtzite and rutile. As the catalyst concentrations increase, the probability of a reaction between dye molecules and catalysts on the sites increases, leading to an enhancement in the decolorization rate; however, at higher concentrations, this rate decreases because of saturation and light transfer problems, especially in single-phase cases. This finding is in agreement with literature reports on the effect of catalyst concentration on treatment efficiency.^{14,15,27,28}

Figure 7 shows the response surface and contour plots of the decolorization efficiency as a function of the concentration of 2 catalyst phases. As can be seen, the decolorization efficiency increases with the adding of a secondary phase to the system. This may be due to the increase of catalyst content in the solution, as reported for single-phase decolorization,^{15,28} with an efficiency decrease from the addition of more catalyst, although, in this case, higher content could be used without losing the efficiency. It could also be due to excessive surface sites, which can increase dye absorption on the surface for formation of hydroxyl radicals, or direct reaction to decompose dye.^{9,29,30}

The effect of secondary phases for anatase and wurtzite are similar, and decolorization efficiency increases rapidly. The enhancement in decolorization efficiency between 2 limits (pure phases) is linear, which can be described with their separate participation in the reaction without a coupling effect.¹⁶

Response optimization and confirmation

The main objective of optimization is to reach higher efficiency with the optimum values of variables from the model obtained using experimental data.^{18,19,31} The optimum values of the reaction parameters for higher

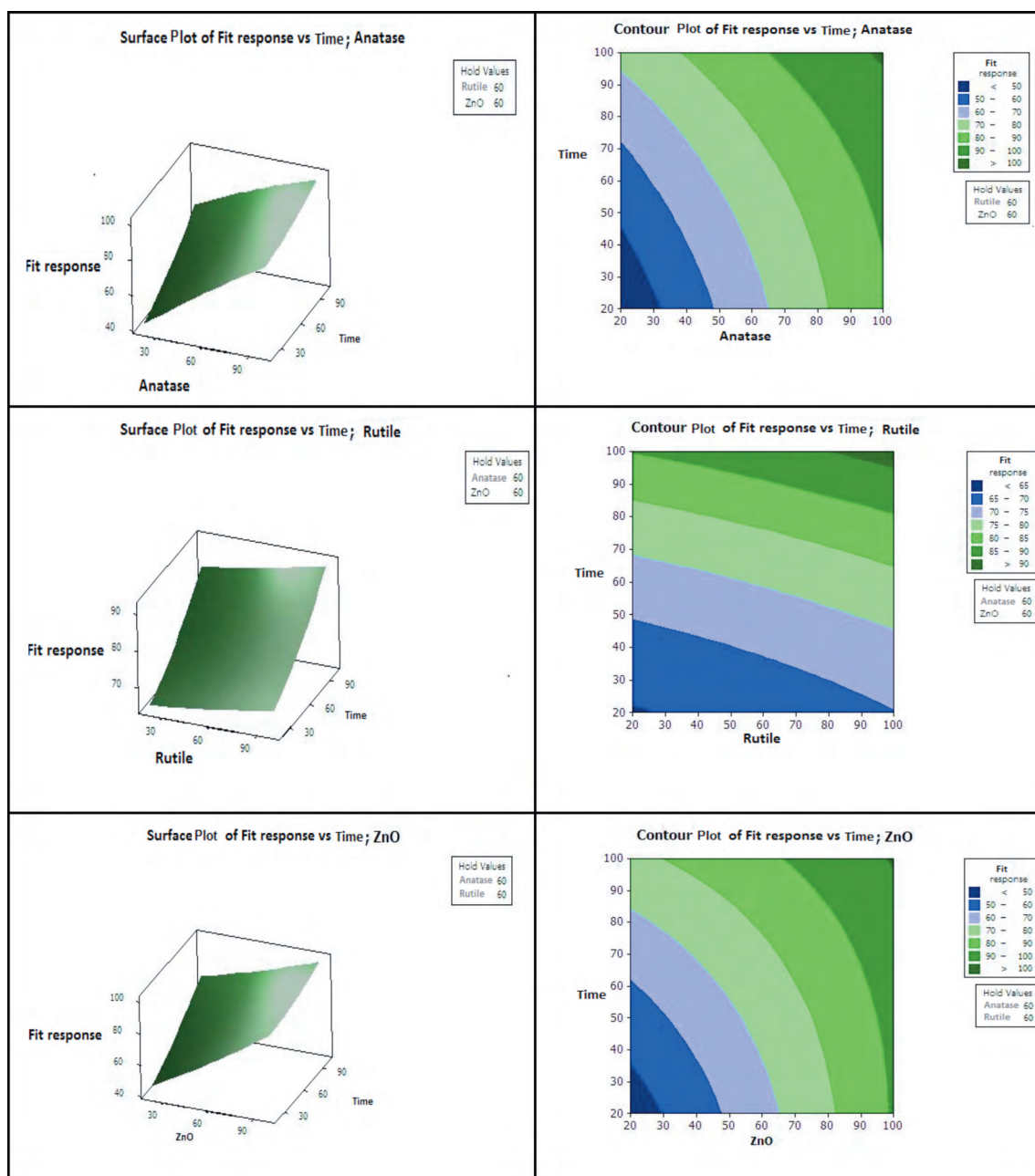


Figure 6. Response surface plot and contour plot of the decolorization efficiency (CR%) as the function of reaction time (min) and catalyst concentrations (ppm) for anatase, rutile, and ZnO, as labeled.

decolorization efficiency are shown in Table 6, implying that this model is useful to optimize the decolorization conditions and to obtain the best conditions by the modeled formula.

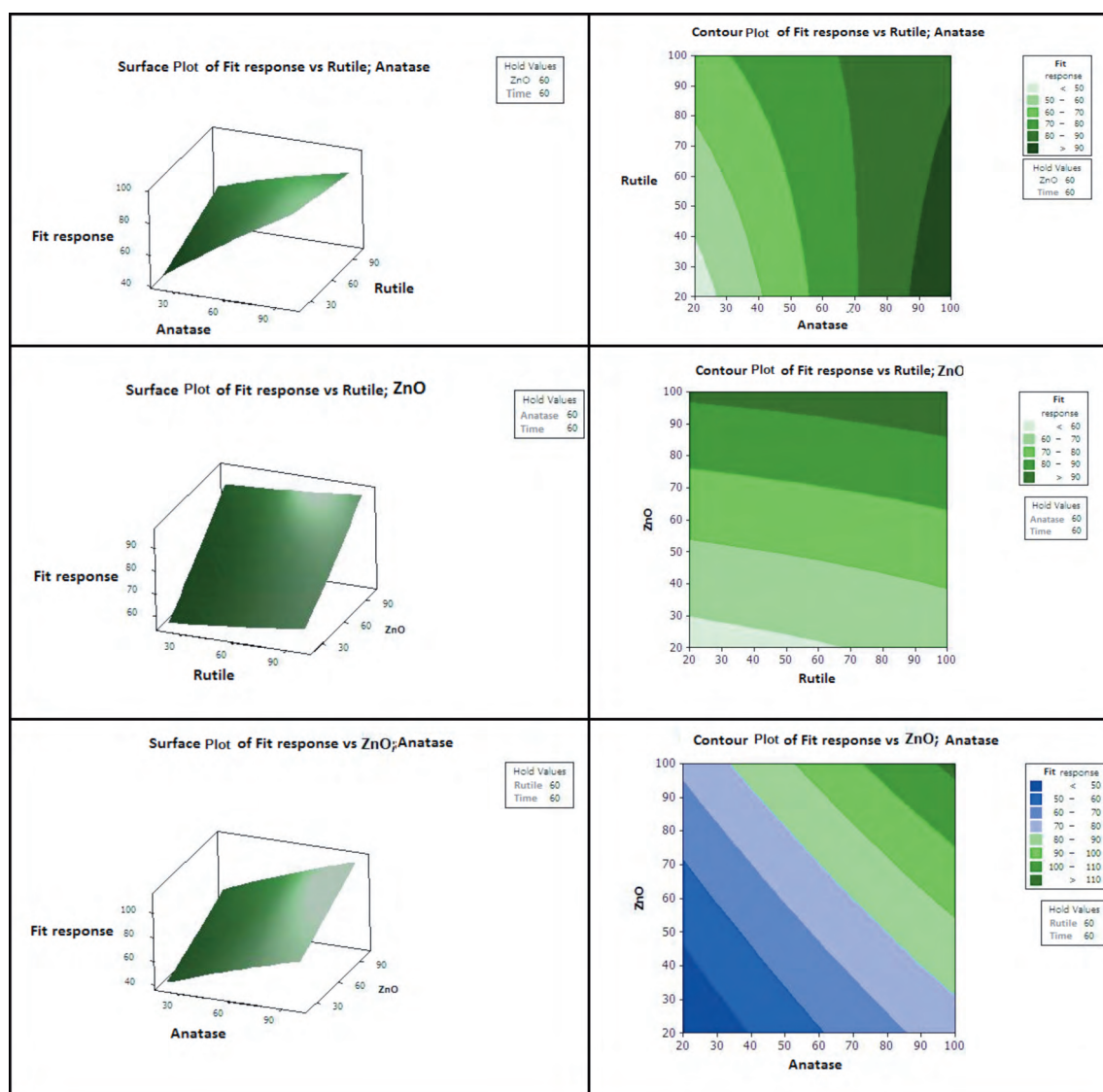


Figure 7. Response surface plot and contour plot of the decolorization efficiency (CR%) as a function of 2 catalyst concentrations (ppm) for rutile/anatase, ZnO/anatase, and ZnO/rutile, as labeled.

Table 6. Optimum values of the process parameters for 99.9% decolorization efficiency.

Variable	Optimum value
Anatase concentration (ppm) (a)	84
Rutile concentration (ppm) (r)	23
ZnO concentration (ppm) (z)	86
Reaction time (min) (t)	48

Conclusions

Photocatalytical decolorization of AR14 was studied by using the CCD mode of RSM. Optimum conditions for this form of an advanced oxidation process could be achieved by setting the experimental parameter modeling. Adjustment of the quadratic model with the experimental data was satisfactory. Analysis of variance showed a high coefficient of determination, in the range of 0.968-0.939. It was possible, therefore, to develop the empirical equations describing and predicting the removal of the dye pollutants. The adjustment and control of the phase's concentrations and use of different catalyst phases were found to be more important for the removal as compared to single-phase cases.

Acknowledgements

The authors thank the Ministry of Science, Research, and Technology of Iran for the financial support provided for S.K.A. to visit METU's Department of Chemical Engineering.

References

1. Banat, I. M.; Nigam, P.; Singh, D.; Marchant, R. *Bioresource Technol.* **1996**, *58*, 217-227.
2. Crini, G. *Bioresource Technol.* **2006**, *97*, 1061-1085.
3. Lachheb, H.; Puzenat, E.; Houas, A.; Ksibi, M.; Elaloui, E.; Guillard, C.; Herrmann, J. M. *Appl. Catal. B Environ.* **2002**, *39*, 75-90.
4. Hachem, C.; Bocquillon, F.; Zahraa, O.; Bouchy, M. *Dyes Pigments* **2001**, *49*, 117-125.
5. Herrmann, J. M. *Catal. Today* **1999**, *53*, 115-129.
6. Chatterjee, D.; Dasgupta, S. *J. Photoch. Photobio. C* **2005**, *6*, 186-205.
7. Osterloh, F. E. *Chem. Mater.* **2008**, *20*, 35-54.
8. Zhao, J.; Yang, X. *Build. Environ.* **2003**, *38*, 645-654.
9. Fujishima, A.; Zhang, X.; Tryk, D. A. *Surf. Sci. Rep.* **2008**, *63*, 515-582.
10. Carp, O.; Huisman, C. L.; Reller, A. *Prog. Solid State Ch* **2004** *32*, 33-177.
11. Pozzo, R. L.; Baltanfis, M. A.; Cassano, A. E. *Catal. Today* **1997**, *39*, 219-231.
12. Ding, Z.; Lu, G. Q.; Greenfield, P. F. *J. Phys. Chem. B* **2000**, *104*, 4815-4820.
13. Hurum, D. C.; Agrios, A. G.; Gray, K. A.; Rajh, T.; Thurnauer, M. C. *J. Phys. Chem. B* **2003**, *107*, 4545-4549.
14. Daneshvar, N.; Salari, D.; Khataee, A. R. *J. Photoch. Photobio. A* **2004**, *162*, 317-322.
15. Daneshvar, N.; Aber, S.; Seyed Dorraji, M. S.; Khataee, A. R.; Rasoulifard, M. H. *Sep. Purif. Technol.* **2007**, *58*, 91-98.
16. Asl, Sh. Kh.; Sadrnezhaad, S. K.; Kianpour rad, M. *Mater. Lett.* **2010**, *64*, 1935-1938.
17. Ohno, T.; Sarukawa, K.; Tokieda, K.; Matsumura, M. *J. Catal.* **2001**, *203*, 82-86.
18. Khataee, A. R.; Zarei, M.; Asl, Sh. Kh. *J. Electroanal. Chem.* **2010**, *648*, 143-150.

19. Fathinia, M.; Khataee, A. R.; Zarei, M.; Aber, S. *J. Mol. Catal. A Chem.* **2010**, *333*, 73-84.
20. Korbahti, B. K.; Rauf, M. A. *Chem. Eng. J.* **2008**, *138*, 166-171.
21. Simpson, T. W.; Peplinski, J. D.; Koch, P. N.; Allen, J. K. *Eng. Comput.* **2001**, *17*, 129-150.
22. Rigas, F.; Panteleos, P.; Laoudis, C. *Global NEST J.* **2000**, *2*, 245-253.
23. Bezerra, M. A.; Santelli, R. E.; Oliveira, E. P.; Villar, L. S.; Escalera, L. A. *Talanta* **2008**, *76*, 965-977.
24. Marchitan, N.; Cojocaru, C.; Mereuta, A.; Duca, Gh.; Cretescu, I.; Gontaa, M. *Sep. Purif. Technol.* **2010**, *75*, 273-285.
25. Bař, D.; Boyacı, İ. H. *J. Food Eng.* **2007**, *78*, 836-845.
26. Bahnemann, D. W.; Hilgendorff, M.; Memming, R. *J. Phys. Chem. B* **1997**, *101*, 4265-4275.
27. Asl, S. K.; Sadrnezhaad, S. K.; Kianpoor rad, M. *Adv. Mat. Res.* **2008**, *55-57*, 577-580.
28. Daneshvar, N.; Salari, D.; Niaei, A.; Khataee, A. R. *J. Environ. Sci. Heal. B* **2006**, *41*, 1273-1290.
29. Zhang, Z.; Wang, C. C.; Zakaria, R.; Ying, J. Y. *J. Phys. Chem. B* **1998**, *102*, 10871-10878.
30. Almquist, C. B.; Biswas, P. *J. Catal.* **2002**, *212*, 145-156.
31. Ahmadi, M.; Vahabzadeh, F.; Bonakdarpour, B.; Mofarrah, E.; Mehranian, M. *J. Hazard. Mater.* **2005**, *123*, 187-195.